RESEARCH ARTICLE

Design and Optimization of Hierarchical Demodulator and Decoder for Layered Coded OFDM-IM With NR-LDPC

ZIJIAN ZENG [1], **HUAN MA** [2], **(Member, IEEE),**
AND LIANG LV [1], **(Graduate Student Member, IEEE)**

[1]School of Information Engineering, Guangdong University of Technology, Guangzhou 510006, China
[2]Electronics and Information Engineering Department, Zhaoqing University, Zhaoqing 526061, China

Corresponding author: Huan Ma (mh-zs@163.com)

ABSTRACT In this paper, we first propose a novel code rate optimized orthogonal frequency division multiplexing with index modulation (OFDM-IM) transceiver architecture based on new radio low-density parity-check (NR-LDPC) coding, referred to as Rate Optimization of Layered Coded OFDM-IM with Hierarchical Demodulator and Decoder (RO-LC-OFDM-IM-HD), which can improve the error performance of system with no spectral efficiency loss. Subsequently, we devise a modified NR-LDPC-based extrinsic information transfer (NR-EXIT) algorithm, to analyze the decoding thresholds of NR-LDPC codes used for index bits and modulation bits in the proposed RO-LC-OFDM-IM-HD. Furthermore, we extend the idea to hierarchical modulation (HM), resulting the rate optimization of multilayered coded HM-OFDM-IM-HD (RO-MLC-HM-OFDM-IM-HD). Simulation results not only indicate that the prosposed RO-LC-OFDM-IM-HD and RO-MLC-HM-OFDM-IM-HD systems outperform the existing counterparts but also are consistent with the theoretical analyses. Therefore, the proposed RO-LC-OFDM-IM-HD and RO-MLC-HM-OFDM-IM-HD systems are competent to provide promising solutions for high reliability and high throughput wireless communications.

INDEX TERMS OFDM with index modulation (OFDM-IM), layered coded, hierarchical demodulator and decoder, NR-LDPC-based extrinsic information transfer (NR-EXIT), hierarchical modulation (HM).

I. INTRODUCTION

With the continuous development of modern information technology, the demand for high throughput and high reliability of wireless communication has become more significant [1]. Some advanced technologies are developed to achieve above requirements. As a multicarrier modulation technique, orthogonal frequency division multiplexing (OFDM) becomes the core technique for 4G and 5G mobile communication systems due to its advantages such as robustness to inter-symbol interference [2], [3]. OFDM is widely used in many modern communication scenarios

The associate editor coordinating the review of this manuscript and approving it for publication was Julien Le Kernec [ID].

such as visible light communications [4] and multiple-input multiple-output communications [5], [6]. One of the major drawbacks of OFDM is its high peak-to-average power ratio (PAPR). Various reduction methods are proposed in [7].

Index modulation (IM) technique can also lower the PAPR [8]. IM is derived from spatial modulation to satisfy the requirements for high spectral efficiency (SE) and energy efficiency (EE) [9], [10]. The classic OFDM with IM (OFDM-IM) has been proposed in [11]. OFDM-IM combines the advantages of OFDM and IM, which provides superior performance against frequency-selective fading [12] and exploits the index of the transmission entities to convey extra information bits [13]. In the OFDM-IM system, the transmitted bits are not only mapped to the subcarriers, but

also mapped to the indicies of the active subcarriers [14]. To further improve SE and system performance, extensive research works have been carried out in [15], [16], [17], and [18]. The in-phase (I-) and quadrature (Q-) dimensions for IM to improve SE have been explored in [15]. The generalized dual-mode IM aided OFDM has been developed to utilize all the subcarriers, in which the symbols are modulated by two distinguishable constellation alphabets in [16]. Furthermore, an extended multiple-mode transmission scheme called multiple-mode OFDM-IM (MM-OFDM-IM) which allows multiple different constellations to be mapped for subcarriers has been discussed in [17]. In [18], a novel framework of OFDM with dual frequency IM (OFDM-DFIM) has been presented to utilize extra bit sequence to jointly determine the active subcarriers. In addition, a low-complexity detector named Greedy detector has also been studied in [19] and [20]. For promising reliability, a simple transmit diversity scheme has been proposed to apply channel coding to the data symbols which can improve the bit error rate (BER) performance, but it only uses channel coding as an auxiliary mean [21].

Low density parity check (LDPC) coding is widely recognized as an effective error correction technique due to its outstanding performance and low decoding complexity [22]. New radio LDPC (NR-LDPC) is a type of quasi-cyclic LDPC (QC-LDPC) codes [23], which can meet the low latency and high throughput requirements in 5G communication systems. By employing LDPC codes in OFDM-IM systems, it enables reliable communication to mitigate the effects of noise interference, such as jamming attacks [24], [25]. Some researchers have evaluated the performance of NR-LDPC-coded OFDM-IM, including OFDM-IM systems and MM-OFDM-IM systems, and indicated that the application of OFDM-IM is limited for LDPC coded scenarios [26]. In recent years, index bits and modulation bits have been separately encoded in [27], which is called coding split [28] OFDM-IM (CS-OFDM-IM) later. A coding split and adjustment (CSA) scheme has been further investigated in [29], which made coded OFDM-IM systems more flexible. However, the correlation between index bits and modulation bits is ignored.

Inspired by the above discussion, we design a novel code rate optimization transceiver of layered coded OFDM-IM with hierarchical demodulator and decoder (RO-LC-OFDM-IM-HD), using NR-LDPC code [30]. The hierarchical structure makes the reliability of modulation bits dependent on detection accuracy of index bits. At the meantime, we optimize the performance of system by utilizing NR-LDPC codes with different code rates for index bits and modulation bits. Additionally, we develop a theoretical analysis tool called NR-LDPC-based extrinsic information transfer (NR-EXIT) to predict the asymptotic convergence performance of the proposed LC-OFDM-IM-HD systems. Furthermore, we extend the idea of code rate optimization to high-order hierarchical modulation (HM) [1], [31], [32], resulting the

rate optimization of multilayered coded OFDM-IM with hierarchical demodulator and decoder (RO-MLC-OFDM-IM-HD) systems. Analytical and simulated results show that the proposed systems have improved error performance.

The remainder of this work is organized as follows. In Section II, we present the system model of RO-LC-OFDM-IM-HD. In Section III, we propose the code rate optimization and develop the NR-EXIT algorithm. In Section IV, the RO-MLC-HM-OFDM-IM-ID system is described and analyzed. The simulation results to demonstrate the superiority of the proposed RO-LC-OFDM-IM-HD and RO-MLC-HM-OFDM-IM-ID systems are provided in Section V. Conclusions are given in VI.

II. SYSTEM MODEL OF RO-LC-OFDM-IM-HD

In this section, we detail the structure of RO-LC-OFDM-IM-HD systems. The code rate optimization would be discussed in Section III. The block diagram of the LC-OFDM-IM-HD transmission system is displayed in Figure 1.

A. TRANSMITTER WITH LAYERED CODING

At transmitter, we consider a layered coded structure. Index information γ_I and modulation information γ_M are separately encoded. The coded index sequence ε_1 of length M_1 and modulation sequence ε_2 of length M_2 are equally divided into Z groups, respectively. For each group, $l_1 = \frac{M_1}{Z}$ index bits are used for index selection and $l_2 = \frac{M_2}{Z}$ modulation bits for classic constellation mapping, such as quadrature amplitude modulation (QAM), phase shift keying (PSK). All N subcarriers of an OFDM symbol are divided into Z subblocks as well, each of which consists of $n = \frac{N}{Z}$ subcarriers. Only k out of n are activated to convey complex symbols. Supposing an M-ary constellation denoted as $\mathbf{Q} = \{Q_1, Q_2, \ldots, Q_M\}$ is employed, we have $l_1 = \lfloor \log_2 C_n^k \rfloor$ and $l_2 = k \times \log_2 M$ in each subblock, where $\lfloor \cdot \rfloor$ is the floor function and C_n^k is the combination function which chooses k elements from n.

The same operations are processed for each subblock, so we consider the b-th subblock as an example. l_1 index bits are mapped to decide k activated subcarriers by using look-up table or one-to-one mapper based on combinatorial method, l_2 modulation bits are mapped into k M-ary symbols. Table 1 provides an optimal combination of subcarriers activation as the look-up table when $n = 4, k = 2$. Denote $\mathbf{I}^b = \{I_1, I_2, \ldots, I_k\}$ as the activated pattern, where $I_k \in \{1, 2, \ldots, n\}$ are the indices of active subcarriers. $\mathbf{C}^b = [C_1, C_2, \ldots, C_n]$ are represented the transmitted symbols, where $C_\alpha \in \mathbf{Q}$ when $\alpha \in \mathbf{I}^b$ and $C_\alpha = 0$ when $\alpha \notin \mathbf{I}^b$. Then, the generated OFDM symbol combined by all subblocks can be given by

$$\mathbf{X} = \left[\mathbf{C}^1, \mathbf{C}^2, \ldots, \mathbf{C}^Z\right]^T = [C_1, C_2, \ldots, C_N]^T. \quad (1)$$

As studied in [17] and [21], interleaved schemes provide better performance by exploiting diversity gain in both
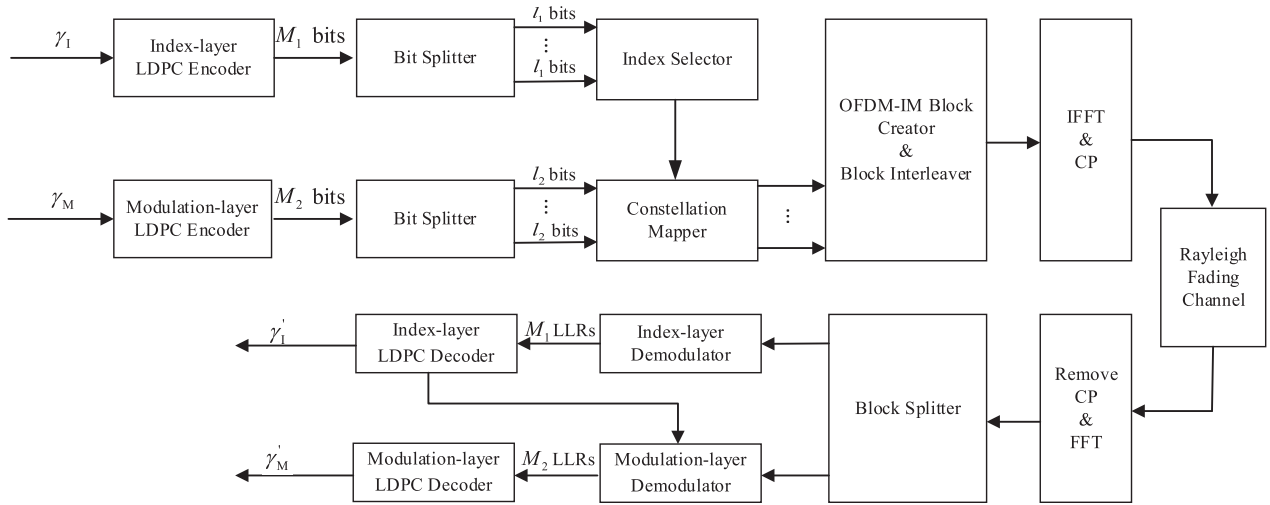
FIGURE 1. Block diagram of the proposed RO-LC-OFDM-IM-HD system.

TABLE 1. A look-up table for $n = 4$, $k = 2$ and $l_1 = 2$.

Index bits	Activated pattern ($\mathbf{I}^b$)
[0 0]	$\{1, 2\}$
[0 1]	$\{1, 3\}$
[1 0]	$\{2, 4\}$
[1 1]	$\{3, 4\}$

uncoded and coded OFDM-IM. Adopting subcarrier inter-leaving, $\mathbf{X}$ can be written as

$$\mathbf{X} = \left[C_1^1, C_1^2, \ldots, C_1^Z, C_2^1, \ldots, C_2^Z, \ldots, C_n^1, \ldots, C_n^Z \right]^T. \tag{2}$$

OFDM processes including Inverse Fast Fourier Transform (IFFT) and adding cyclic prefix (CP) are then performed, where the length of IFFT and CP are N and N_{CP}, respectively.

B. RECEIVER WITH HIERARCHICAL DEMODULATOR AND DECODER

The symbols pass through a frequency-selective Rayleigh fading channel. We assume that N_{CP} is larger than maximum time domain latency $d_{\max}$, and channel state information (CSI) is perfectly estimated at receiver. After CP removal, FFT and de-interleaving, output vector can be written as

$$\mathbf{Y} = \mathbf{HX} + \mathbf{A}, \tag{3}$$

where $\mathbf{H} = diag\{h_1, h_2, \ldots, h_N\}$ is the frequency domain channel matrix whose diagonal elements follow the complex Gaussian distribution $\mathcal{CN}(0, 1)$ and $\mathbf{A} = [a_1, a_2, \ldots, a_N]^T$ is the AWGN vector whose elements follow $\mathcal{CN}(0, N_0)$, where N_0 is the noise power spectral density. In addition, the average signal power per constellation symbol is assumed to be E_s, hence the signal-to-noise ratio (SNR) is equal to E_s/N_0.

At the receiver, soft information LLR is needed for LDPC decoding. According to the layered coded transmitter

described in Section II-A, we proposed a hierarchical demodulator and decoder (HD) structure. Because the calculation of bit LLRs for each subblock is independent of the other subblocks, based on the maximum likelihood (ML) algorithm, the LLRs of l_1 index bits and l_2 modulation bits in the b-th subblock can be respectively defined as

$$\beta(\rho_{\text{I}}(j)) = \ln \frac{P(\rho_{\text{I}}(j) = 0|\mathbf{y}_b)}{P(\rho_{\text{I}}(j) = 1|\mathbf{y}_b)}, \tag{4}$$

$$\beta(\rho_{\text{M}}(l)) = \ln \frac{P(\rho_{\text{M}}(l) = 0|\mathbf{y}_b)}{P(\rho_{\text{M}}(l) = 1|\mathbf{y}_b)}, \tag{5}$$

where $j = 1, 2, \ldots, l_1$, $l = 1, 2, \ldots, l_2$. Assume the a priori probability of the coded bits are equal. Therefore we first calculate the index bit LLRs which can be rewritten as

$$\beta(\rho_{\text{I}}(j)) = \ln \frac{P(\mathbf{y}_b|\rho_{\text{I}}(j) = 0)}{P(\mathbf{y}_b|\rho_{\text{I}}(j) = 1)} = \ln \frac{\sum\limits_{\rho_{\text{I}}(j)=0,\mathbf{I}^b} \sum\limits_{\mathbf{Q}^b} P(\mathbf{y}_b|\mathbf{x}_b)}{\sum\limits_{\rho_{\text{I}}(j)=1,\mathbf{I}^b} \sum\limits_{\mathbf{Q}^b} P(\mathbf{y}_b|\mathbf{x}_b)}, \tag{6}$$

where $\mathbf{x}_b = [x_1, x_2, \ldots, x_n]^T$ is jointly determined by $\mathbf{I}^b$ and $\mathbf{Q}^b$ which consists of k complex signals selected from $\mathbf{Q}$. Then we have

$$P(\mathbf{y}_b|\mathbf{x}_b) = \prod_{i=1}^{n} \exp(-\frac{|y_i - h_i x_i|^2}{N_0}), \tag{7}$$

where x_i, y_i, h_i are the symbols at transmitter and receiver, the channel coefficient of the i-th subcarrier in the b-th subblock.

Similarly, modulation bit LLRs can be computed by the same process detailed above. However, if n and k are larger, the calculation will get burdened. Therefore, we then decode the index bits by soft-decision based on the LLRs from (6). Subsequently, a detected activated pattern $\mathbf{I}'$ for each subblock can be obtained by mapping decoded index sequence ε_1'. Finally, the LLRs of modulation bits can be formulated as follows. Depending on the detected activated

subcarriers determined by $\mathbf{I}'$, we have a simplified calculation method as

$$
\begin{aligned}
\beta(\rho_{\mathrm{M}}(l)) &= \ln \frac{P(\mathbf{y}_b|\rho_{\mathrm{M}}(l)=0)}{P(\mathbf{y}_b|\rho_{\mathrm{M}}(l)=1)} \\
&= \ln \frac{\sum\limits_{\mathbf{I}';\,\rho_{\mathrm{M}}(l)=0,\mathbf{Q}^b} P(\mathbf{y}_b|\mathbf{x}_b)}{\sum\limits_{\mathbf{I}';\,\rho_{\mathrm{M}}(l)=1,\mathbf{Q}^b} P(\mathbf{y}_b|\mathbf{x}_b)}.
\end{aligned}
\tag{8}
$$

Here $\mathbf{x}_b$ is jointly determined by $\mathbf{I}'$ and $\mathbf{Q}^\mathbf{b}$. The modulation bit LLRs are fed into corresponding decoder and decoded modulation sequence ε_2' is outputted. The log-domain belief propagation (log-BP) decoding algorithm is used for both LDPC decoders. Decoded index information γ_{I}' and modulation information γ_{M}' are separated from ε_1' and ε_2'.

III. CODE RATE OPTIMIZATION AND NR-EXIT ALGORITHM

A. NR-LDPC CODE

NR-LDPC code from 3GPP standard is employed for our schemes because of its flexibility and accuracy of code rate. The encoding process of NR-LDPC code involves multiplying the information bits with the parity check matrix. This matrix is generated by base graph (BG) and lifting factors (Z_c). 3GPP standard prescribes two types of BGs and provides a lifting factor table. Moreover, a BG corresponds to a base matrix $\mathbf{B} = (p_{i,j})$ of size $m_c \times n_v$, where m_c and n_v are the numbers of check nodes (CNs) and variable nodes (VNs), respectively. To achieve different coding rates, a technique called rate matching is employed to NR-LDPC codes. This involves puncturing, shortening and zero padding bits in the codeword to achieve the desired rate.

B. CODE RATE OPTIMIZATION

The detection accuracy of index bits depends mainly on the Hamming distance for the index bits of different index combinations, while the detection accuracy of modulation bits relies on Euclidean distance of the constellation symbols. There is significant error performance difference between index bits and modulation bits in CS-OFDM-IM [27]. In order to improve the system reliability, we proposed the code rate optimization based on the LC-OFDM-IM-HD system, resulting RO-LC-OFDM-IM-HD. In detail, because the detection accuracy of index bits makes a significant impact on the detection of modulation bits when HD is used, we employed LDPC codes with lower code rate (R_{I}) for index bits and increase the code rate (R_{M}) of the modulation bits accordingly. For fair comparison, we should ensure the proposed system spectral efficiency is equal to that of CS-OFDM-IM system. Thus, several examples of code rate combinations from low to high are provided in Table 2, R_{A} denotes the average code rate which corresponds to classic scheme. Taking N_{CP} into account, the SE can be calculated by

$$
\delta = \frac{(R_{\mathrm{I}} l_1 + R_{\mathrm{M}} l_2) \times Z}{N + N_{\mathrm{CP}}} \quad (\text{bit/s/Hz}),
\tag{9}
$$

where N_{cp} is set to a quarter of the number of subcarriers $N/4$.

TABLE 2. Code rate combination for the RO-LC-OFDM-IM-HD and corresponding Spectral efficiency.

R_{A}	(n,k)	R_{I}	R_{M}	SE (bit/s/Hz)
0.4	(4,1)	0.36	0.44	0.32
	(4,2)	0.26	0.47	0.48
	(4,3)	0.2	0.467	0.64
0.6	(4,1)	0.57	0.63	0.48
	(4,2)	0.5	0.65	0.72
	(4,3)	0.39	0.67	0.96
0.8	(4,1)	0.79	0.81	0.64
	(4,2)	0.8	0.8	0.96
	(4,3)	0.71	0.83	1.28

C. NR-EXIT ALGORITHM AND CONVERGENCE ANALYSIS

In order to investigate the convergence performance of the proposed NR-LDPC-coded RO-LC-OFDM-IM-HD system, we modified the protograph EXIT (PEXIT) algorithm [1] for NR-LDPC as the asymptotic performance analysis tool, called NR-EXIT algorithm. We analyzed the decoding thresholds of index bits and modulation bits, respectively. The mutual information (MI) passing procedure is presented in Figure 2, where we define the following related notations.

1) $I_{\mathrm{Ed,I}}(j)$ and $I_{\mathrm{Ed,M}}(j)$ denote the extrinsic MIs of v_j for index bits and modulation bits from the OFDM-IM hierarchical demodulator, respectively;
2) $I_{\mathrm{Av}}(i,j)$ and $I_{\mathrm{Ac}}(i,j)$ denote the a-priori MIs passed from c_i to v_j and v_j to c_i, respectively;
3) $I_{\mathrm{Ev}}(i,j)$ and $I_{\mathrm{Ec}}(i,j)$ denote the extrinsic MIs passed from v_j to c_i and c_i to v_j, respectively;
4) $I_{\mathrm{AP}}(j)$ denotes the a-posteriori MI of v_j;

where c_i and v_j denote the i-th CN and j-th VN ($i = 1, 2, \ldots, m_c, j = 1, 2, \ldots, n_v$), respectively.
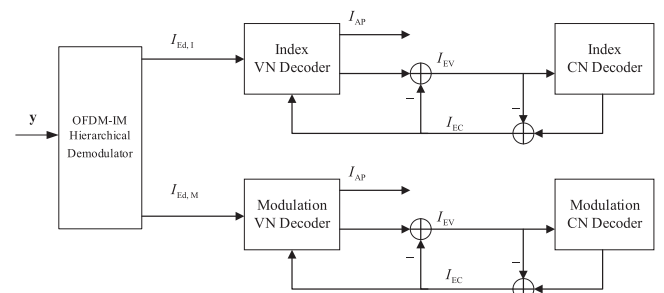

FIGURE 2. Flow chart of the NR-EXIT algorithm for LDPC-coded RO-LC-OFDM-IM-HD system.

As described in [33], the function $J(\cdot)$ and its inverse function $J^{-1}(\cdot)$ determine the conversion relationship between MI and standard deviation σ_{ch} when the channel LLRs of coded bits follow a Gaussian distribution $\beta \sim \mathcal{N}(\sigma_{\mathrm{ch}}^2/2, \sigma_{\mathrm{ch}}^2)$. Hence, the NR-EXIT can be briefly illustrated as follows.

1) Initialization: An initial SNR value and a maximum number of iteration $\mathcal{T}$ are set for Monte-Carlo

simulation. OFDM symbols from channel are passed into the hierarchical OFDM-IM demodulator for LLR calculation.

2) The extrinsic MIs of index bits and modulation bits calculation: After index demodulation, coded index bit LLRs have been accomplished. In particular, we complete the punctured bits and padded zero bits LLRs by assigning former as 0 and latter as positive infinity. Aforementioned extrinsic LLRs are used to calculate the extrinsic MIs of v_j $I_{Ed,I}(j)$ for LDPC of index coded sequence. Specifically, $I_{Ed,I}$ can be calculated as

$$I_{Ed,I}(j) = 1 - E\left[\log_2(1 + e^{-\varepsilon_{1,k}^c \beta_k^I})\right], \quad (10)$$

where $E[\cdot]$ is the expectation function, $\varepsilon_{1,k}^c$ and β_k^I denote the k-th converted index binary symbol and corresponding LLR, respectively. And $\varepsilon_{1,k}^c \in \{1, -1\}$ is formulated by

$$\varepsilon_{1,k}^c = (-1)^{\varepsilon_{1,k}}, \quad (11)$$

where $\varepsilon_{1,k} \in \{0, 1\}$ denotes the k-th coded index bit and $k = (j-1)Z_c + 1, (j-1)Z_c + 2, \ldots, jZ_c$. Similarly, according to modulation bit $\varepsilon_{2,k}$ and its LLR β_k^M, the extrinsic MIs $I_{Ed,M}$ for LDPC of modulation coded sequence can be calculated as

$$I_{Ed,M}(j) = 1 - E\left[\log_2(1 + e^{-\varepsilon_{2,k}^c \beta_k^M})\right], \quad (12)$$

$$\varepsilon_{2,k}^c = (-1)^{\varepsilon_{2,k}}. \quad (13)$$

The following steps are the same for LDPC codes of index bits and modulation bits so we only describe index part to illustrate.

3) Passing extrinsic MIs to VNs: The initial decoding MIs are set as $I_{init}(j) = I_{Ed,I}(j)$. Specially, $I_{init}(j) = 0$ if v_j is a punctured VN and $I_{init}(j) = 1$ when all the bits of v_j after a Z_c-lifting are padding zeros.

4) Updating the extrinsic MIs from VNs: Based on $I_{init}(j)$ and the a priori MI $I_{Av}(i, j)$, the extrinsic MI $I_{Ev}(i, j)$ can be updated when bit in column j of row i $b_{i,j} \neq 0$ in base graph. And $I_{Ac}(i, j) = I_{Ev}(i, j)$.

5) Updating the extrinsic MIs from CNs: According to the a priori MI $I_{Ac}(i, j)$, the corresponding extrinsic MI $I_{Ec}(i, j)$ can be updated when $b_{i,j} \neq 0$ in base graph. Then we use $I_{Av}(i, j) = I_{Ec}(i, j)$ for the next iteration.

6) The a posteriori MIs for VNs calculation: Exploiting $I_{Av}(i, j)$ and $I_{init}(j)$, we can compute the a posteriori MI $I_{AP}(j)$.

7) Decision: If $I_{AP}(j) = 1$ for $j = 1, 2, \ldots, n_v$, the algorithm terminates and we consider that it is able to be decoded successfully at current SNR and think this SNR value is the decoding threshold. On the other hand, the algorithm restarts with a smaller increment of SNR if the iteration number reaches $\mathcal{T}$. Otherwise, return to step 4 for next iteration.

By simulating with a 0.01 dB SNR increment, the decoding thresholds of index bits and modulation bits in various cases

of Table 2 are shown in Table 3. We compare the decoding thresholds of the CS-OFDM-IM as well. We can observe the decoding thresholds of the RO-LC-OFDM-IM-HD become lower compared with the CS-OFDM-IM, especially for modulation bits.

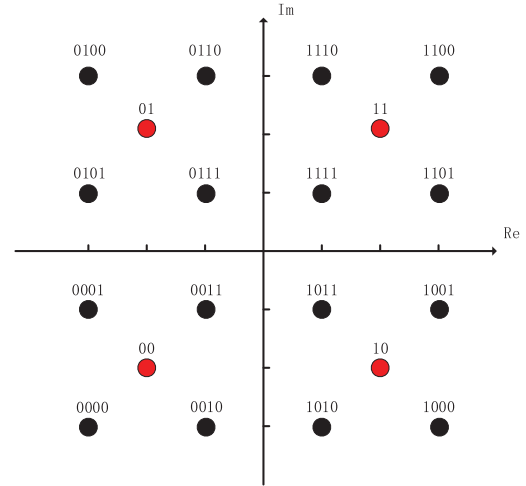## IV. MLC-HM-OFDM-IM-HD SYSTEMS AND ASYMPTOTIC CONVERGENCE ANALYSIS

FIGURE 3. Gray constellation for HM-based 16-QAM.

A. HM-BASED M-QAM

For higher-order QAM modulation, each constellation symbol is mapped by multiple bits, e.g. $\log_2 16 = 4$ bits for 16-QAM, and $\log_2 64 = 6$ bits for 64-QAM. From the results in [1], there are differences in the error performance of information at different layers using hierarchical modulation (HM). To facilitate the understanding of the HM process, a specific example based on Gray constellation is given in Figure 3. The main idea can be simply elaborated as the 4-bit 16-QAM constellation is mapped through two layers. The first 2 bits are used as the first layer (modulation-1) to determine the quadrant where the constellation point is located. The last two bits act as the second layer (modulation-2), which determines the position in the corresponding quadrant and the whole constellation according to Gray rule. Layered structure of HM can provide unequal error protection (UEP) for different information.

From another point of view, according to the design of HM, we extended the idea of the code rate optimization to the OFDM-IM system of high-order HM-QAM, resulting the RO-MLC-HM-OFDM-IM-HD system. Specifically, taking 16-QAM as an example, the two layers of information in HM are encoded separately, and the information of the index layer is encoded individually, which are a total of three independent layers of coding. This design can split the original modulation layer longer LDPC code into two shorter LDPC codes, which is easy to implement. At the same time, we use the hierarchical demodulator and decodor structure described in Section II-B, which can simplify the calculation

TABLE 3. Decoding thresholds of LDPC codes used for the index bits and modulation bits under 4-QAM in the existing CS-OFDM-IM systems and the proposed RO-LC-OFDM-IM-HD systems.

R_A	(n,k)	CS-OFDM-IM (dB)		RO-LC-OFDM-IM-HD (dB)		
		Index bits	Modulation bits	Code rate combination	Index bits	Modulation bits
0.4	(4,1)	-2.11	-2.38	(0.36,0.44)	-2.4	-2.81
	(4,2)	-0.17	0.4	(0.26,0.47)	-2.1	-1.57
	(4,3)	3.18	1.91	(0.20,0.467)	0.45	0.64
0.6	(4,1)	0.33	0.35	(0.57,0.63)	0.04	-0.09
	(4,2)	2.06	3.12	(0.50,0.65)	0.95	1.45
	(4,3)	5.41	4.94	(0.39,0.67)	3.13	3.92
0.8	(4,1)	2.92	3.34	(0.79,0.81)	2.76	2.78
	(4,2)	4.68	6.34	(0.80,0.80)	4.71	5.05
	(4,3)	8.02	8.27	(0.71,0.83)	6.92	7.47
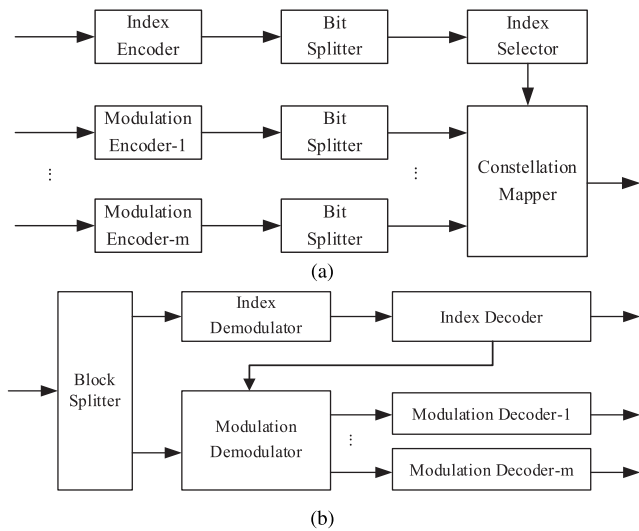
FIGURE 4. The block diagram of (a) the transmitter and (b) the receiver in MLC-HM-OFDM-IM-HD.

FIGURE 5. Gray constellation for HM-based 64-QAM.

of the LLRs of modulation bits. Figure 4 illustrates the MLC transmitter and the HD receiver of the RO-MLC-HM-OFDM-IM-HD system. Here we omit the part from OFDM-IM block creator to block splitter, which is the same as Figure 1. The design of MLC can provide more flexibility for code rate optimization. We optimize the code rate combination of the three codes to obtain better average bit error performance of the system while ensuring that the average code rate remains equal. For fair comparison, the MLC-HM structure is introduced into the CS-OFDM-IM and the LC-OFDM-IM-HD, resulting the CS-MLC-HM-OFDM-IM and the MLC-HM-OFDM-IM-HD.

B. NR-EXIT ANALYSIS FOR RO-MLC-HM-OFDM-IM-HD SYSTEM

For the proposed RO-MLC-HM-OFDM-IM-HD system, we provide the optimal code rate combination when $n = 4, k = 1$. The asymptotic convergence performance of the three-layer coding of the system is analyzed by using the NR-EXIT algorithm in Section III-C. The code rates of all layers for the CS-MLC-HM-OFDM-IM and the MLC-HM-OFDM-IM are 0.5. The code rates of index bits, modulation-1 bits and modulation-2 bits for the
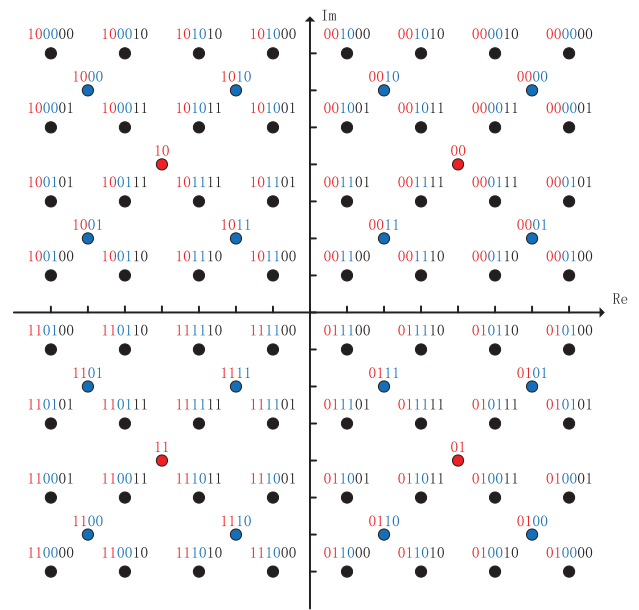
RO-MLC-HM-OFDM-IM-HD are 0.5, 0.6 and 0.4, respectively. The obtained decoding thresholds are shown in Table 4 and compared with the CS-MLC-HM-OFDM-IM system and the MLC-HM-OFDM-IM-HD system without code rate optimization. For the CS-MLC-HM-OFDM-IM system and the MLC-HM-OFDM-IM-HD system, the decoding thresholds of modulation-2 bits is more higher than index bits and modulation-1 bits. By exploiting the code rate optimization, the decoding thresholds of index bits and modulation-1 bits are slightly decreased and increased, respectively. The decoding threshold of modulation-2 bits is decreased obviously. This plays a significant role in the average error performance of the system.

In addition, we provided the HM-based 64-QAM Gray constellation in Figure 5, which consists of 6 bits and is divided into three layers (modulation-1, modulation-2, modulation-3) according to the order of 2 bits in each layer.. Similarly, we also performed the NR-EXIT analysis on 64-QAM system when $n = 4, k = 1$. The code rates of index bits, modulation-1 bits, modulation-2 bits and modulation-3

TABLE 4. Decoding thresholds of LDPC codes used for various layers in the CS-MLC-HM-OFDM-IM system, the MLC-HM-OFDM-IM-HD system and the RO-MLC-HM-OFDM-IM-HD system with 16-QAM.

	System	Index bits	Modulation-1 bits	Modulation-2 bits
	CS	1.22dB	1.33dB	3.59dB
Decoding thresholds	MLC	1.25dB	1.15dB	2.58dB
	RO-MLC	0.97dB	1.27dB	1.36dB

TABLE 5. Decoding thresholds of LDPC codes used for various layers in the CS-MLC-HM-OFDM-IM system, the MLC-HM-OFDM-IM-HD system and the RO-MLC-HM-OFDM-IM-HD system with 64-QAM.

	System	Index bits	Modulation-1 bits	Modulation-2 bits	Modulation-3 bits
	CS	1.12dB	2.06dB	6.37dB	8.89dB
Decoding thresholds	MLC	1.11dB	1.10dB	5.62dB	8.71dB
	RO-MLC	3.31dB	3.64dB	4.61dB	5.35dB

bits for the RO-MLC-HM-OFDM-IM-HD are 0.62, 0.67, 0.43 and 0.28, respectively. Results are shown in Table 5. We can come to a similar conclusion that the decoding thresholds of modulation-2 bits and modulation-3 bits have noticeable reduction though the decoding thresholds of index bits and modulation-1 bits are increased. This is mainly beacause we have to increase the code rates of index bits and modulation-1, when we achieve lower decoding thresholds of modulation-2 and modulation-3 bits by decreasing their code rates. But the average error performance of the system is always determined by the worst layer, especially at higher SNR region. Hence, the improvement of the performance is significant.

V. SIMULATION RESULTS

In this section, to prove the merit of the proposed systems, we provide various bit-error-rate (BER) simulation results over Rayleigh fading channel. Unless otherwise specified, we assume the total number of subcarriers for an OFDM symbol is 1024. The maximum number of decoding iteration is set to 20.

A. BER PERFORMANCE FOR THE 4-QAM SYSTEMS

We evaluate the system error performance of the proposed RO-LC-OFDM-IM-HD, and validate the superiority of the design of code rate optimization by comparing with other existing schemes. We simulate different code rates and activated subcarrier numbers with 4-QAM. The optimized code rate combinations are provided in Table 2. The code length of index bits is 512 and code lengths of modulation bits are 512, 1024, 1536 when $n = 4$, $k = 1, 2, 3$, respectively.

Figure 6 depicts the index bits BER (IBER) and modulation bits BER (MBER) curves of the CS-OFDM-IM, the proposed LC-OFDM-IM-HD and the RO-LC-OFDM-IM-HD systems when $R = 0.6$. There are significant differences between IBER and MBER of the CS-OFDM-IM. On the other hand, the gaps between them become smaller when the proposed HD receiver is used. For $k = 1$, the CS-OFDM-IM achieves IBER and MBER of 10^{-5} at SNRs of 3.97 dB and 4.55 dB. Similarly, the CS-OFDM-IM requires SNRs of 5.09 dB and
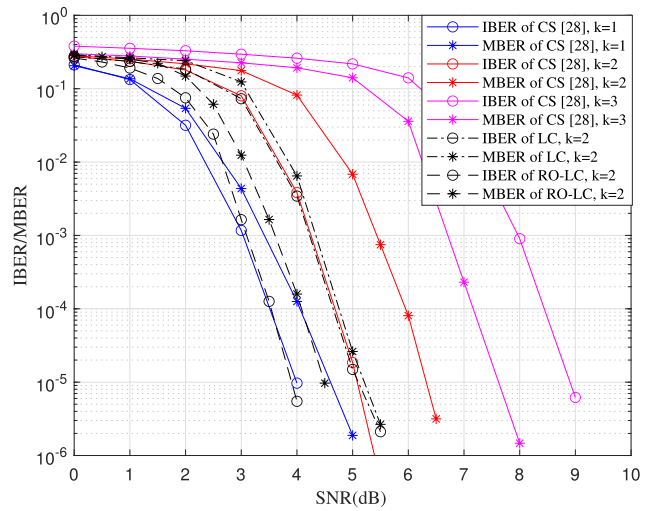

FIGURE 6. IBER and MBER curves of the CS-OFDM-IM when $n = 4$, $k = 1, 2, 3$, the proposed LC-OFDM-IM-HD and RO-LC-OFDM-IM-HD when $n = 4$, $k = 2$.

6.30 dB to do so when $k = 2$, while corresponding SNRs for k=3 are 8.90 dB and 7.62 dB, respectively. We clearly observe that MBER is better than IBER when $k = 3$ rather IBERs are better than MBERs when $k = 1$ and $k = 2$. This is because if code rate remains constant, the LDPC of longer code length provides better the error correction performance. For $R = 0.6$ and $k = 2$, the LC-OFDM-IM-HD requires SNRs of about 5.09 dB and 5.20 dB to achieve the IBER and MBER of 10^{-5}. Moreover, the RO-LC-OFDM-IM-HD with $R = 0.6$ and $k = 2$ achieves the IBER and MBER of 10^{-5} at lower SNRs of 3.87 dB and 4.52 dB. The above results confirm our proposed hierarchical structure makes MBER dependent on IBER.

Figure 7 shows the average BER (ABER) curves of the LDPC coded classic OFDM-IM, the CS-OFDM-IM, the proposed LC-OFDM-IM-HD and the RO-LC-OFDM-IM-HD for $R = 0.4, 0.6, 0.8$ when $n = 4$, $k = 1$. We compare the error performance at the ABER level of 10^{-5} as well. The LC-OFDM-IM-HD has different performance comparison with the classic OFDM-IM when R is changed. The ABER of
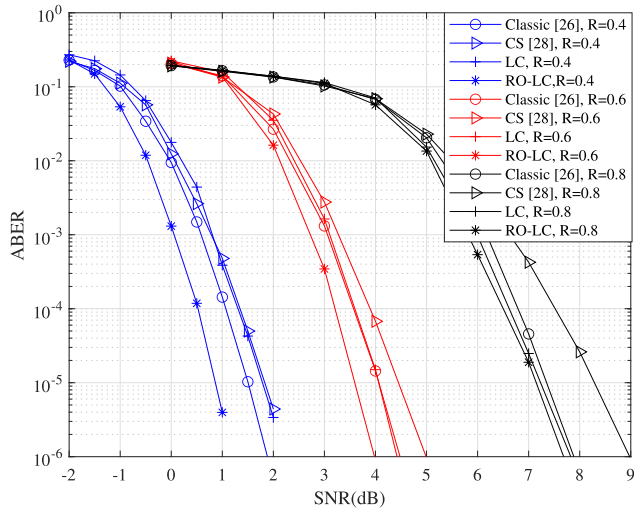
FIGURE 7. ABER curves of the classic OFDM-IM, the CS-OFDM-IM, the proposed LC-OFDM-IM-HD, and the RO-LC-OFDM-IM-HD systems for $R = 0.4, 0.6, 0.8$ when $k = 1$.
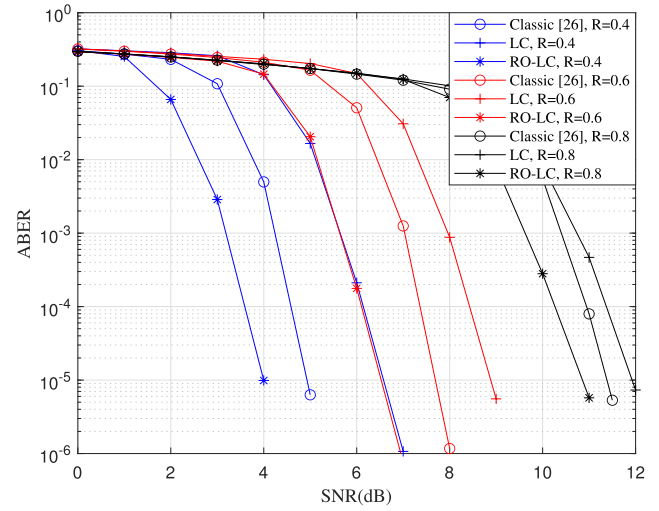

FIGURE 9. ABER curves of the classic OFDM-IM, the proposed LC-OFDM-IM-HD, and the RO-LC-OFDM-IM-HD systems for $R = 0.4, 0.6, 0.8$ when $k = 3$.
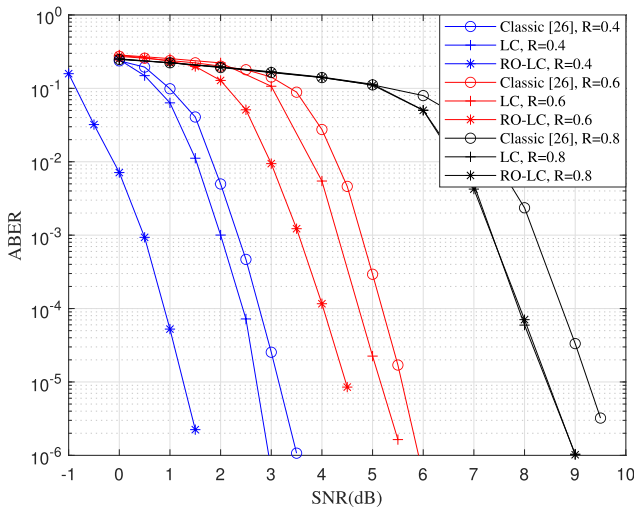

FIGURE 8. ABER curves of the classic OFDM-IM, the proposed LC-OFDM-IM-HD, and the RO-LC-OFDM-IM-HD systems for $R = 0.4, 0.6, 0.8$ when $k = 2$.

the LC-OFDM-IM-HD is 0.28 dB worse than the classic OFDM-IM when $R = 0.4$, gets very close to the classic OFDM-IM when $R = 0.6$, and is 0.13 dB better when $R = 0.8$. Taking the classic OFDM-IM as the benchmark, the LC-OFDM-IM-HD has better performance as R increases. The RO-LC-OFDM-IM-HD obtains about 0.67 dB gain over the classic OFDM-IM and 0.96 dB over the CS-OFDM-IM for $R = 0.4$. Similarly, the corresponding gains for $R = 0.6$ are 0.50 dB and 0.86 dB, for $R = 0.8$ are 0.20 dB and 1.12 dB, respectively. The RO-LC-OFDM-IM-HD always achieves optimal performance among these four schemes.

From the previous simulation results, the classic OFDM-IM usually performs better than the CS-OFDM-IM in various R. Therefore, we only compare the performance of the classic OFDM-IM, the LC-OFDM-IM-HD and the RO-LC-OFDM-IM-HD in the following simulations. We simulate the ABER curves of the above three OFDM-IM systems with

different R for $k = 2$, and present the results in Figure 8. We can observe that the LC-OFDM-IM-HD performs better than the classic OFDM-IM in the case of $k = 2$, which can achieve the gains of 0.43 dB, 0.5 dB and 0.81 dB when $R = 0.4, 0.6, 0.8$, respectively. The gains become larger as the R increases. The RO-LC-OFDM-IM-HD obtains more significant gains over the classic OFDM-IM, which are about 1.91 dB, 1.09 dB and 0.82 dB for $R = 0.4, 0.6, 0.8$, respectively. Specially, the LC-OFDM-IM-HD and the RO-LC-OFDM-IM-HD are almost the same when $R = 0.8$. Because the RO-LC-OFDM-IM-HD obtains the optimal performance when R_I and R_M are almost identical to 0.8.

Figure 9 depicts the ABER curves of three schemes with $k = 3$. Similarly, the RO-LC-OFDM-IM-HD performs by about 0.92 dB, 1.21 dB and 0.55 dB over the classic OFDM-IM for $R = 0.4, 0.6, 0.8$, respectively. But the LC-OFDM-IM-HD has worse ABER compared with the classic OFDM-IM. However, taking the classic OFDM-IM as benchmark, it is apparent that the LC-OFDM-IM-HD maintains the same trend as Figure 7 and Figure 8 that it performs better as the R increases. Above simulation results imply that our proposed HD structure is suitable to layered coded OFDM-IM systems. Moreover, the proposed RO-LC-OFDM-IM-HD exhibits the best performance among all OFDM-IM systems.

B. BER PERFORMANCE FOR THE HM-BASED QAM SYSTEMS

In the case of $n = 4$ and $k = 1$, we simulate the BER performance of the CS-MLC-HM-OFDM-IM system, the MLC-HM-OFDM-IM-HD system without code rate optimization and the RO-MLC-HM-OFDM-IM-HD system. The HM-based 16-QAM in Figure 3 and 64-QAM in Figure 5 are applied. Similarly, the subcarrier number of OFDM is set to 1024, hence the index bits code length and the modulation bits code length of each layer are 512. The
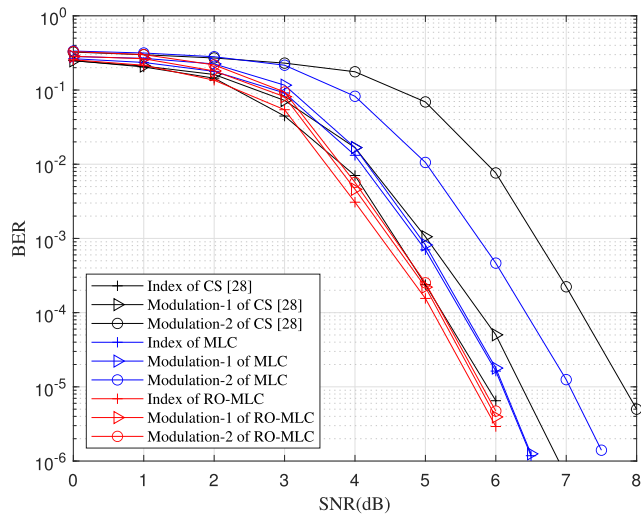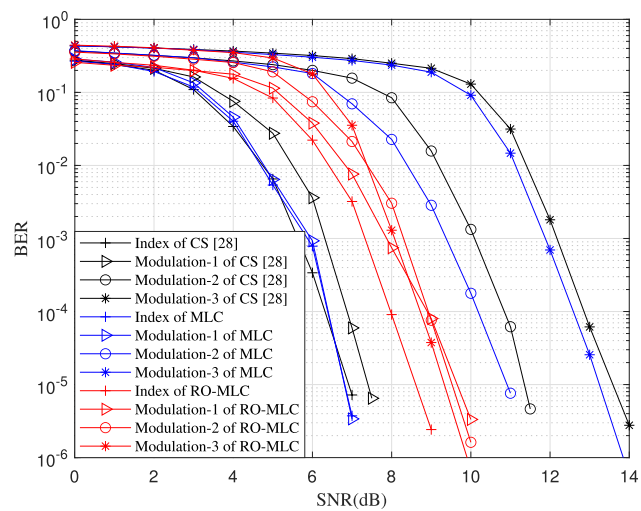
FIGURE 10. BER curves of different layers in the CS-MLC-HM-OFDM-IM, the MLC-HM-OFDM-IM-HD and the RO-MLC-HM-OFDM-IM-HD, with (a) 16-QAM and (b) 64-QAM.

FIGURE 11. ABER curves of the CS-MLC-HM-OFDM-IM, the MLC-HM-OFDM-IM-HD, and the RO-MLC-HM-OFDM-IM-HD systems with 16-QAM and 64QAM.

at the ABER level of 10^{-5}, respectively. And the RO-MLC-HM-OFDM-IM-HD performs by about 1.82dB and 3.74dB over the CS-MLC-HM-OFDM-IM under 16-QAM and 64-QAM, respectively.

VI. CONCLUSION

In this paper, we have proposed a RO-LC-OFDM-IM-ID system to boost the error performance without spectral efficiency loss. Based on the system, we have also developed a modified NR-EXIT algorithm to analyse the convergence performance of the NR-LDPC codes used for index bits and modulation bits, respectively. Theoretical analysis results have demonstrated that the proposed RO-LC-OFDM-IM-HD possesses desirable decoding thresholds. Meanwhile, simulation results have indicated that RO-LC-OFDM-IM-HD achieves superior BER performance compared with other existing LDPC coded OFDM-IM. Subsequently, we have extended the idea of RO to the HM-based QAM. The both results have proved the merit of the RO-MLC-HM-OFDM-IM-HD system. Additionally, the impacts on decoding speeds of the RO-LC-OFDM-IM-HD and the RO-MLC-HM-OFDM-IM-HD are minimal. Thanks to the aforementioned advantages, we believe our proposed RO-LC-OFDM-IM-HD and RO-MLC-HM-OFDM-IM-HD systems can be considered as promising alternatives for the future high-throughput communication scenarios.

code rate combination for different layers are given in Section IV.

As we can see from Figure 10, the BER of various layers of 16-QAM and 64-QAM are different in the MLC-HM-OFDM-IM-HD without code rate optimization and the CS-MLC-HM-OFDM-IM. Obviously, the BER of 16-QAM modulation-2 layer information and 64-QAM modulation-3 layer information in both the CS-MLC-HM-OFDM-IM and the MLC-HM-OFDM-IM-HD are the worst, which directly determine the average error performance of the whole system. Compared with the other two systems, the gap between BER of various layers in the RO-MLC-HM-OFDM-IM-HD become smaller. Figure 11 shows the ABER curves of the CS-MLC-HM-OFDM-IM, the MLC-HM-OFDM-IM-HD and the RO-MLC-HM-OFDM-IM-HD systems with 16-QAM and 64-QAM. The RO-MLC-HM-OFDM-IM-HD can obtain gains of 1.01dB and 3.49 dB compared with the MLC-HM-OFDM-IM-HD under 16-QAM and 64-QAM modulation
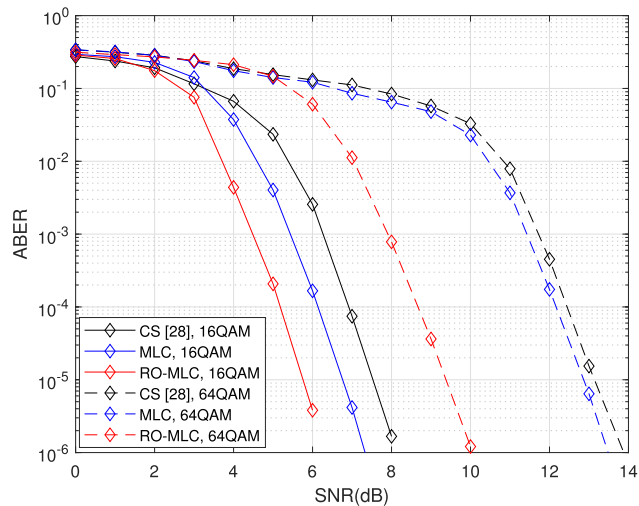
REFERENCES

[1] Z. Yang, Y. Fang, G. Han, and K. M. S. Huq, "Spatially coupled protograph LDPC-coded hierarchical modulated BICM-ID systems: A promising transmission technique for 6G-enabled Internet of Things," *IEEE Internet Things J.*, vol. 8, no. 7, pp. 5149–5163, Apr. 2021.

[2] A. T. Dogukan, O. F. Tugtekin, and E. Basar, "Coordinate interleaved OFDM with power distribution index modulation," *IEEE Commun. Lett.*, vol. 26, no. 8, pp. 1908–1912, Aug. 2022.

[3] J. Yang, Y. Fang, L. Dai, P. Chen, and G. Han, "Residual network-based channel estimation for the protograph LDPC-coded OFDM systems," *IEEE Commun. Lett.*, vol. 27, no. 10, pp. 2568–2572, Oct. 2023.

[4] L. Dai, Y. Fang, P. Chen, G. Zhang, and M. Guizani, "A new transceiver design for protograph LDPC-coded LACO-OFDM VLC systems with deep learning," *IEEE Commun. Lett.*, vol. 27, no. 3, pp. 896–900, Mar. 2023.

[5] G. Femenias and F. Riera-Palou, "Wideband cell-free mmWave massive MIMO-OFDM: Beam squint-aware channel covariance-based hybrid beamforming," *IEEE Trans. Wireless Commun.*, vol. 21, no. 7, pp. 4695–4710, Jul. 2022.

[6] T. Murakami, R. Taniguchi, T. Ogawa, and Y. Takatori, "Performance evaluation of uplink multiuser MIMO-OFDM system with single RF chain receiver," *IEEE Access*, vol. 10, pp. 118878–118887, 2022.

[7] M. El Hassan, M. Crussière, J.-F. Hélard, Y. Nasser, and O. Bazzi, "EVM closed-form expression for OFDM signals with tone reservation-based PAPR reduction," *IEEE Trans. Wireless Commun.*, vol. 19, no. 4, pp. 2352–2366, Apr. 2020.

[8] N. Ishikawa, S. Sugiura, and L. Hanzo, "Subcarrier-index modulation aided OFDM–will it work?" *IEEE Access*, vol. 4, pp. 2580–2593, 2016.

[9] Y. Fang, D. Peng, H. Ma, G. Han, and Y. Li, "A neural network-aided detection scheme for index-modulation DCSK system," *IEEE Trans. Veh. Technol.*, vol. 73, no. 2, pp. 2109–2121, Feb. 2024.

[10] Y. Fang, J. Zhuo, H. Ma, M. Shahid, and Y. Li, "Design and analysis of a new index-modulation-aided DCSK system with frequency-and-time resources," *IEEE Trans. Veh. Technol.*, vol. 72, no. 6, pp. 7411–7425, Aug. 2023.

[11] E. Basar, Ü. Aygölü, E. Panayirci, and H. V. Poor, "Orthogonal frequency division multiplexing with index modulation," *IEEE Trans. Signal Process.*, vol. 61, no. 22, pp. 5536–5549, Nov. 2013.

[12] H. Ma, Y. Fang, P. Chen, and Y. Li, "Reconfigurable intelligent surface-aided M-ary FM-DCSK system: A new design for noncoherent chaos-based communication," *IEEE Trans. Veh. Technol.*, vol. 72, no. 4, pp. 4829–4843, Apr. 2023.

[13] H. Ma, Y. Fang, G. Cai, G. Han, and Y. Li, "A new frequency-bin-index LoRA system for high-data-rate transmission: Design and performance analysis," *IEEE Internet Things J.*, vol. 9, no. 14, pp. 12515–12528, Jul. 2022.

[14] H. Ma, Y. Fang, P. Chen, S. Mumtaz, and Y. Li, "A novel differential chaos shift keying scheme with multidimensional index modulation," *IEEE Trans. Wireless Commun.*, vol. 22, no. 1, pp. 237–256, Jan. 2023.

[15] M. Wen, B. Ye, E. Basar, Q. Li, and F. Ji, "Enhanced orthogonal frequency division multiplexing with index modulation," *IEEE Trans. Wireless Commun.*, vol. 16, no. 7, pp. 4786–4801, Jul. 2017.

[16] T. Mao, Q. Wang, and Z. Wang, "Generalized dual-mode index modulation aided OFDM," *IEEE Commun. Lett.*, vol. 21, no. 4, pp. 761–764, Apr. 2017.

[17] M. Wen, E. Basar, Q. Li, B. Zheng, and M. Zhang, "Multiple-mode orthogonal frequency division multiplexing with index modulation," *IEEE Trans. Commun.*, vol. 65, no. 9, pp. 3892–3906, Sep. 2017.

[18] X. Ning, B. Zhang, and Z. Wang, "OFDM with dual frequency index modulation," *IEEE Commun. Lett.*, vol. 26, no. 3, pp. 617–621, Mar. 2022.

[19] T. Van Luong and Y. Ko, "A tight bound on BER of MCIK-OFDM with greedy detection and imperfect CSI," *IEEE Commun. Lett.*, vol. 21, no. 12, pp. 2594–2597, Dec. 2017.

[20] T. Van Luong and Y. Ko, "Impact of CSI uncertainty on MCIK-OFDM: Tight closed-form symbol error probability analysis," *IEEE Trans. Veh. Technol.*, vol. 67, no. 2, pp. 1272–1279, Feb. 2018.

[21] J. Choi, "Coded OFDM-IM with transmit diversity," *IEEE Trans. Commun.*, vol. 65, no. 7, pp. 3164–3171, Jul. 2017.

[22] L. Dai, Y. Fang, Y. L. Guan, and M. Guizani, "Design of protograph LDPC-coded MIMO-VLC systems with generalized spatial modulation," *China Commun.*, vol. 99, pp. 1–17, 2023.

[23] Y. Fang, G. Han, G. Cai, F. C. M. Lau, P. Chen, and Y. L. Guan, "Design guidelines of low-density parity-check codes for magnetic recording systems," *IEEE Commun. Surveys Tuts.*, vol. 20, no. 2, pp. 1574–1606, 2nd Quart., 2018.

[24] A. Kaplan, M. Can, I. Altunbas, G. K. Kurt, and D. Kucukyavuz, "LDPC coded OFDM-IM performance evaluation under jamming attack," in *Proc. Int. Conf. Inf. Commun. Technol. Converg. (ICTC)*, Oct. 2020, pp. 69–74.

[25] A. Kaplan, M. Can, I. Altunbas, G. K. Kurt, and D. Kucukyavuz, "Comparative performance evaluation of LDPC coded OFDM-IM under jamming attack," *IEEE Trans. Veh. Technol.*, vol. 72, no. 5, pp. 6209–6224, May 2023.

[26] X. Yu and J. Pang, "Performance evaluation of OFDM index modulation with LDPC code," in *Proc. IEEE Annu. Int. Sym. Pers. Indoor Mobile Radio Commu.*, Sep. 2020, pp. 1–5.

[27] Y. Chen, T. Xu, and I. Darwazeh, "Index modulation pattern design for non-orthogonal multicarrier signal waveforms," *IEEE Trans. Wireless Commun.*, vol. 21, no. 10, pp. 8507–8521, Oct. 2022.

[28] Y. Chen, C. Wang, J. Si, and T. Xu, "Anti-eavesdropping and anti-jamming waveform design with coding split index modulation," in *Proc. IEEE/CIC Int. Conf. Commun. China (ICCC)*, Aug. 2023, pp. 1–6.

[29] Y. Chen, W. Yuan, and T. Xu, "Coding split and adjustment to defend OFDM-IM against jamming attacks," *IEEE Commun. Lett.*, vol. 27, no. 2, pp. 457–461, Feb. 2023.

[30] *3GPP: TS 38.212 NR; Multiplexing and Channel Coding*, 3rd Generaation Partnership Project (3GPP), Sophia Antipolis, France, 2018.

[31] H. Alasti and S. Gazor, "Vectored implementation of hierarchical 2^{2n} QAM," *IEEE Trans. Circuits Syst. II, Exp. Briefs*, vol. 62, no. 11, pp. 1103–1107, Nov. 2015.

[32] H. Méric, J. Lacan, F. Arnal, G. Lesthievent, and M.-L. Boucheret, "Combining adaptive coding and modulation with hierarchical modulation in Satcom systems," *IEEE Trans. Broadcast.*, vol. 59, no. 4, pp. 627–637, Dec. 2013.

[33] Z. Yang, Y. Fang, G. Zhang, and F. C. M. Lau, "Design and optimization of protograph LDPC-coded multipulse PPM systems over Poisson channels," *IEEE Trans. Veh. Technol.*, vol. 71, no. 9, pp. 9586–9601, Sep. 2022.

ZIJIAN ZENG was born in Maoming, China, in 1998. He received the B.Sc. degree in communication engineering from Guangdong University of Technology, China, in 2021, where he is currently pursuing the M.Sc. degree in communication engineering.

His current research interests include LDPC codes, index modulation, and OFDM communication.

HUAN MA (Member, IEEE) received the B.Sc. degree in communication engineering from Heilongjiang University, Harbin, China, in 2017, and the M.Sc. degree in electronic and communication engineering and the Ph.D. degree in communication engineering from Guangdong University of Technology, Guangzhou, China, in 2020 and 2023, respectively.

He is currently a Lecturer with the Electronics and Information Engineering Department, Zhaoqing University, Zhaoqing, China. His research interests include spread-spectrum modulation, reconfigurable intelligent surface, and the Internet of Things.

LIANG LV (Graduate Student Member, IEEE) received the B.Sc. degree in communication engineering from Suqian University, China, in 2020, and the M.Sc. degree in communication engineering from Guangdong University of Technology, China, in 2023. He is currently pursuing the Ph.D. degree with the School of Information Engineering, Guangdong University of Technology, China.

His research interests include channel coding and modulation, wireless communications, and free-space optical communications.